Liquid Crystals
Publication details, including instructions for authors and subscription information:
http://www.informaworld.com/smpp/title~content=t713926090

Mass transport in a chiral nematic/nematic liquid crystal system

H. Hakemi[ab]
[a] Corporate Research Division, Louis Laboratory, S.C. Johnson and Son, Inc., Racine, Wisconsin, U.S.A.
[b] Specialty Polymer Department, Eniricerche S.p.A., S. Donato Milanese, Milan, Italy

To cite this Article Hakemi, H.(1988) 'Mass transport in a chiral nematic/nematic liquid crystal system', Liquid Crystals, 3: 4, 453 — 468
To link to this Article: DOI: 10.1080/02678298808086394
URL: http://dx.doi.org/10.1080/02678298808086394

LIQUID CRYSTALS, 1988, VOL. 3, NO. 4, 453–468

Mass transport in a chiral nematic/nematic liquid crystal system

by H. HAKEMI†
Corporate Research Division, Louis Laboratory, S.C. Johnson and Son, Inc., Racine, Wisconsin 5303, U.S.A.

(*Received 23 March 1987; accepted 7 December 1987*)

The optical microscopic mass transport technique has been used to study diffusion phenomenon in a chiral nematic/nematic solute/solvent mixture. Analysis of the concentration–distance, concentration–time and distance–time of the diffusion profile gave the diffusion coefficient of the system as a function of time, distance and concentration, respectively. The mutual diffusion coefficient of the system was independent of the distance and time, showing an average value of $2{\cdot}65 \times 10^{-7}\,cm^2\,s^{-1}$. In non-steady state diffusion, the diffusion coefficient was dependent on both distance and time. The diffusion coefficient exhibited an inverse relation with the local concentration of the chiral solute. The self-diffusion coefficient of the nematic solvent gave a value of $3{\cdot}4 \times 10^{-7}\,cm^2\,s^{-1}$ via extrapolation to zero concentration of the solute.

1. Introduction

Diffusion phenomena in liquids have been the subject of extensive theoretical and experimental studies. A comprehensive review of this subject has recently been published [1]. There exist a number of well-developed and accurate experimental techniques for the evaluation of diffusion coefficients in fluid systems. These techniques are based either on macroscopic (mass transport) or microscopic (N.M.R., light scattering, etc.) approaches.

In the mass transport techniques, the diffusion coefficient of the system is determined by the decay of a macroscopic concentration gradient in either a binary or a multicomponent solute/solvent mixture. Depending on the nature and the molecular structure of the components, the mutual (inter-) diffusion or the tracer (intra-) diffusion coefficients of a system may be determined. The physical foundation and the mathematical formulation of these mass transport approaches are based on the Fick's laws of diffusion. In the microscopic techniques, however, with the absence of bulk concentration gradient, both the tracer and the self-diffusion coefficients can be determined from the transient relaxation or the time-average autocorrelation functions. The physical concepts of this approach are based on the molecular fluctuations and the brownian motion concepts, where the corresponding mathematical formulations are based on random walk statistics.

Although the exact relation between the diffusion coefficients obtained by these two approaches is not yet completely understood, the physical foundations of diffusion by the molecular fluctuations and the fickian concepts are the same. Both approaches result into the same mathematical formulation which is referred to as the diffusion equation. In one dimension, the diffusion equation is described by the

† Present address: Specialty Polymer Department, Eniricerche S.p.A., 20097 S. Donato Milanese, Milan, Italy.

differential equation [2]

$$\partial c/\partial t = \partial/\partial x(D\ \partial c/\partial x), \quad (1)$$

where D is the diffusion coefficient and x is the penetration distance of the solute with concentration c at time t. When D is assumed to be constant, equation (1) is further simplified to

$$\partial c/\partial t = D(\partial^2 c/\partial x^2). \quad (2)$$

Although in equation (2), D is assumed to be independent of x and t, its independence from c is not implicit in this equation. In both macroscopic and microscopic techniques, determination of the diffusion coefficient from equation (2) is based on a linear relation between the concentration gradient and the material flux. The concentration gradient may be of the macroscopic or the microscopic scale. Accordingly, the interpretation of D depends on the nature of the experimental method and the evaluation of the diffusion coefficient. In mass transport studies of liquids, evaluation of the diffusion coefficient is based on the measurement of the concentration distribution as a function of the penetration distance or diffusion time. For one-dimensional diffusion, there are only three fundamental experimental parameters of concentration c (or its equivalent value), distance x and time t. Accordingly, a one-dimensional diffusion profile may be shown by a three dimensional surface bound to a c–x–t cartesian coordinate system (see § 4).

In spite of the diversity of the mass transport techniques in liquids [1], they all are limited to the measurement of the diffusion coefficients in either the c–x frame (at constant t) or the c–t frame (at constant x). None of the conventional mass transport methods are capable of providing the analysis of the diffusion profile in the x–t frame (at constant c). Considering the recent experimental developments of the optical microscopic mass transport technique (OMMT) in both thermotropic [3–6] and lyotropic [7, 8] liquid-crystalline systems, no attempt has yet been made to analyse the c–x–t diffusion surface and determine the corresponding diffusion coefficients. In the present study we have determined the diffusion coefficients in a chiral nematic/nematic system as a function of time, distance and concentration. From a dynamic analysis of the c–x–t diffusion surface, we found that above a characteristic space–time value the diffusion was in the steady state. We have determined both the differential and the integral values of the diffusion coefficient in the mesomorphic system. In this experiment, since the uniaxial orientation of the nematic director and the cholesteric helix axis was obtained only by the surface treatment, the effect of the diffusion anisotropy was averaged over the helical pitch within the whole range of the concentration gradient (see [4(e)].

2. Experimental

The materials used in this study were nematic 4-*n*-pentyl-4′-cyanobiphenyl (5CB), and its chiral isomer 4-(2′-methyl)butyl-4′-cyanobiphenyl (CB15). 5CB exhibits a nematic phase within the temperature range 22 to 35°C, whereas the non-mesomorphic CB15 has a virtual cholesteric phase below −30°C. The compounds were obtained from BDH Chemicals Ltd and were used without further purification. The diffusion cell consisted of an optical precision glass container with outside dimensions of 0·9 × 4·5 cm and an inside thickness of 5×10^{-3} cm.

The diffusion path was prepared by placing the 5CB nematic solvent between the treated surfaces of the optical cell. The surfaces were coated with polyvinyl-alcohol (PVA) and rubbed unidirectionally to induce a homogeneous (parallel) alignment in the nematic film. The diffusion profile was established by allowing a small droplet of a 4·95 per cent (w/w) chiral nematic (cholesteric) solution of CB15/5CB to diffuse linearly into the uniaxial nematic solvent. The diffusion cell was placed into a specially designed microscopic hot stage using a Brinkmann Lauda RM6 temperature control circulator and the temperature was kept constant at 24 $\pm$ 0·5°C during the diffusion process. The liquid-crystalline texture of the diffusion profile was monitored under a Zeiss Universal polarizing microscope equipped with a calibrated microscale, and the space–time behaviour of the diffusion texture was measured directly. The method of analysis and the experimental details of this technique have been described elsewhere [3, 4]. The overall experimental error in these experiments is within $\pm$ 10 per cent.

3. Evaluation of the helical pitch and the concentration

Figure 1 shows the photomicrographs of the time evolution of the diffusion profile in the CB15/5CB system. According to the surface treatment, the average cholesteric helical axis is oriented perpendicular to the glass surfaces. The observed pitch gradient in the diffusion texture experiences discontinuous jumps at locations where sharp structural defects (or disclination lines) occur (see figure 1). However, the actual or undisturbed helical pitch (which is modified by the concentration gradient) is subject to continuous changes [4(c), 4(e)]. The exact relation between the undisturbed pitch and the concentration of the chiral solute in dilute solutions is given by [9, 10]

$$p_k = \gamma/c_k, \tag{3}$$

where p_k is the undisturbed pitch of the solution at the concentration c_k, and γ is the proportionality constant whose value depends on the molecular structure, temperature and the extent of the liquid crystal–surface interactions.

In the presence of a concentration gradient, the relation between the undisturbed pitch and the film thickness is given by [3(b)]

$$p_k = 2d/k, \tag{4}$$

where $k = 1, 2, 3, \ldots$, represent the locations of the corresponding p_k at the mid-distance between the observed successive disclination lines (figure 1). Since, during the relaxation of the pitch gradient, p_k values at the mid-distance points should remain constant, evaluation of the undisturbed pitch values at the disclination lines is also possible. At each disclination line, the observed pitch is subjected to a discontinuous change from k to $k + 1$, whereas the actual pitch changes continuously. Consequently, by knowing the x values at the disclination lines, their corresponding undisturbed pitch values were determined by interpolation from p_k versus x plots. For simplicity we designate the undisturbed pitch at the disclination lines by $p_{k-1,k}$, i.e. at $k = 1, 2, 3, \ldots$ they are presented by $p_{01}, p_{12}, p_{23} \ldots$, respectively. The exact values of p_k and $p_{k-1,k}$ are tabulated in the table.

Determination of the concentrations attributed to the p_k and $p_{k-1,k}$ values was carried out in two steps. First, we calibrated equation (3) by calculating γ. This

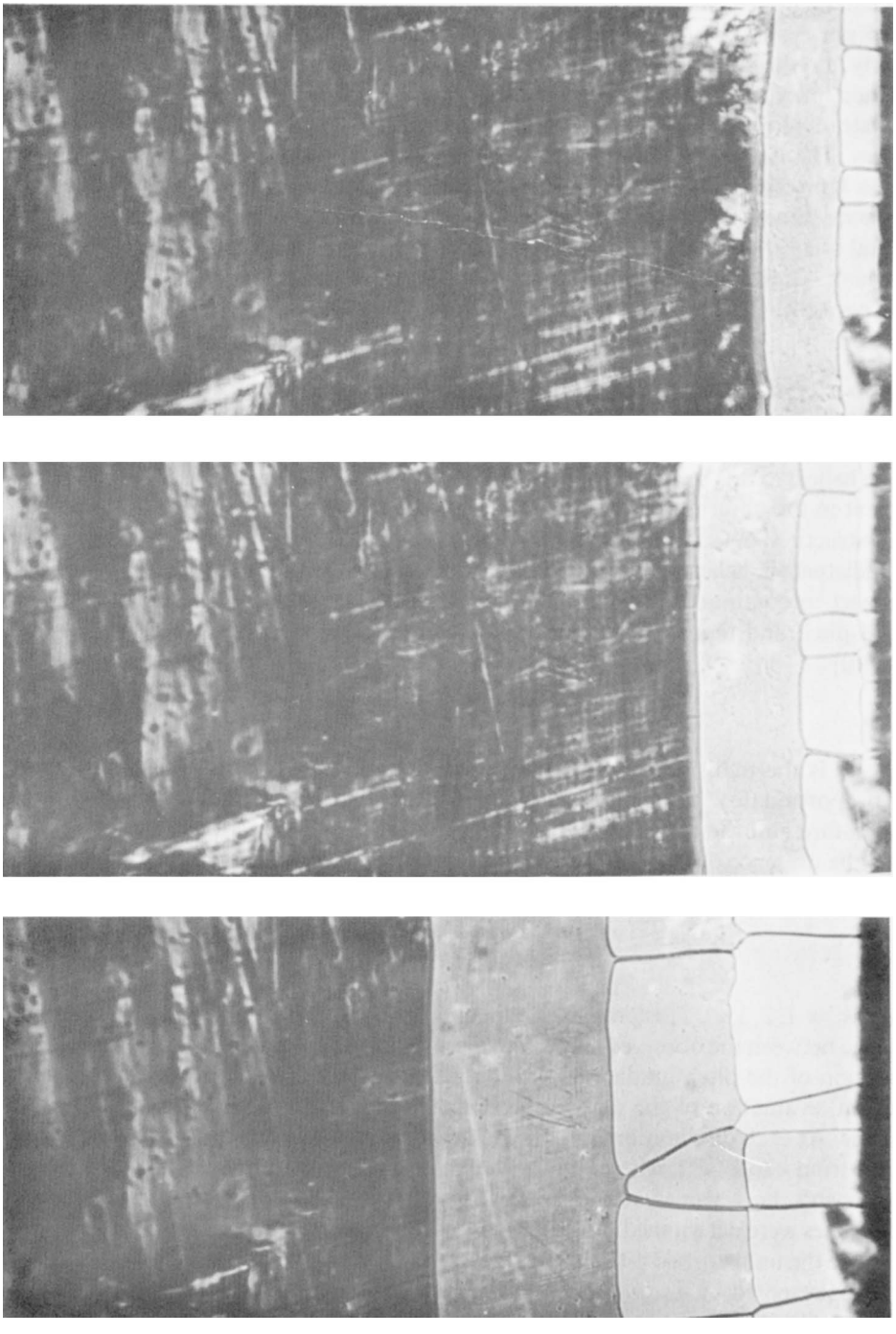

Figure 1. The time evolution (from right to left) of diffusion texture of the CB15/5CB system observed under a polarizing microscope. The diffusion direction is from bottom to top. Magnification = ×60.

Pitch and concentration values in the diffusion profile of CB15/5CB at $d = 5 \times 10^{-3}$ cm and $T = 23{\cdot}5°C$.

				$D_{xt}/10^7\,cm^2\,s^{-1}$	
n	k $(k-1, k)$	$p/10^4$ cm	$c/10^3\,g\,ml^{-1}$	Slope	Curve fitting
1	$(0 \rightarrow 1)$	152	2·00	3·20	3·30
2	1	100	3·05	3·20	3·25
3	$(1 \rightarrow 2)$	63·5	4·80	2·80	2·75
4	2	50	6·15	2·80	2·80
5	$(2 \rightarrow 3)$	40	7·65	2·60	2·40
6	3	33·5	9·15	2·50	2·45
7	$(3 \rightarrow 4)$	27·5	11·10	2·30	2·20
8	4	25	12·25	2·20	2·15
9	$(4 \rightarrow 5)$	22	13·85	2·20	1·90
10	5	20	15·30	2·10	1·70
11	$(5 \rightarrow 6)$	17·5	17·50	1·80	1·25
12	6	15·6	18·35	1·80	1·40
13	$(6 \rightarrow 7)$	16	19·15	1·50	1·00
		$p_0 = 6{\cdot}2$	$c_0 = 49{\cdot}5$		

was done by substituting the initial concentration $c_0 = 4{\cdot}95$ per cent (w/w) and its corresponding pitch $p_0 = 6{\cdot}2 \times 10^{-4}$ cm in equation (3), which gave $\gamma = 3{\cdot}1 \times 10^{-3}$ cm. The p_0 value was obtained from a recent pitch measurement study on the CB15/5CB system [11]. Secondly, the calibrated equation (3) was used to evaluate the concentrations attributed to p_k, $p_{k-1,k}$ values. The calculated concentrations for CB15/5CB diffusion profile are also given in the table.

4. Determination of the diffusion coefficients

The mathematical solution to equation (2) for the semi-infinite boundary condition in one dimension is the gaussian relaxation [2]

$$c = [M/(\pi Dt)^{1/2}]\exp(-x^2/4Dt), \tag{5}$$

where x and t are the space and time coordinates of the solute with concentration c, M is the total amount of the diffusing solute and D is the mutual diffusion coefficient of the system which is assumed to be independent of space, time and concentration. In general, however, a diffusion coefficient which is not integrated over x, t and c is not expected to be constant. Note that all the reported literature data on the concentration dependence of D refer to the total concentration of the solute (either the initial c or the difference between the initial and final c) rather than the differential or local concentrations in the diffusion profile.

According to equation (5), it is possible to select three experimental conditions for the analysis of the diffusion profile from a three-dimensional c–x–t surface. In figure 2, we show the solution of equation (5) on a cartesian coordinate system. The c–x–t surface can be analysed experimentally on individual c–x, c–t and x–t planes. By proper choice of the experimental constants and variables and by rearrangements of the corresponding parameters in equation (5), the analysis of the c–x–t diffusion surface and the calculation of the corresponding diffusion coefficients can be carried

out from the equations

$$\ln[c] = \ln[M/(\pi D_{cx}t)^{1/2}] - (1/4D_{cx}t)[x^2], \quad (6)$$

$$\ln[c(t^{1/2})] = \ln[M/(\pi D_{ct})^{1/2}] - (x^2/4D_{ct})[t^{-1}], \quad (7)$$

$$[x^2/t] = 2D_{xt}\ln[M^2/D_{xt}c^2] - 2D_{xt}\ln[t], \quad (8)$$

where D_{cx}, D_{ct} and D_{xt} are the diffusion coefficients measured in the corresponding experimental frames. From equations (6), (7) and (8), we determined the corresponding diffusion coefficients as a function of time, distance and concentration in the CB15/5CB system.

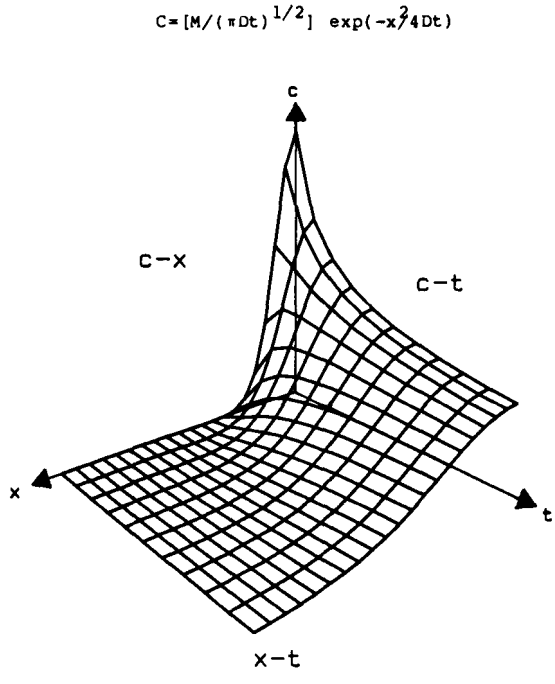

Figure 2. An example of a c–x–t diffusion surface in a cartesian coordinate system calculated from equation (5).

5. Results and discussion

5.1. *Diffusion coefficient versus time*

According to figure 2 and equation (6), the time variation of the diffusion coefficient D_{cx} can be studied by the analysis of the data on the c–x planes as a function of time. In figure 3, we show the time evolution of the concentration distribution in CB15/5CB system for a series of c versus x curves. The behaviour of these curves clearly demonstrate the gaussian-type relaxations of the spatial distribution of the concentrations. In agreement with the diffusion boundary condition, the data also show the transient depletion of the solute concentration at the diffusion source ($x = 0$).

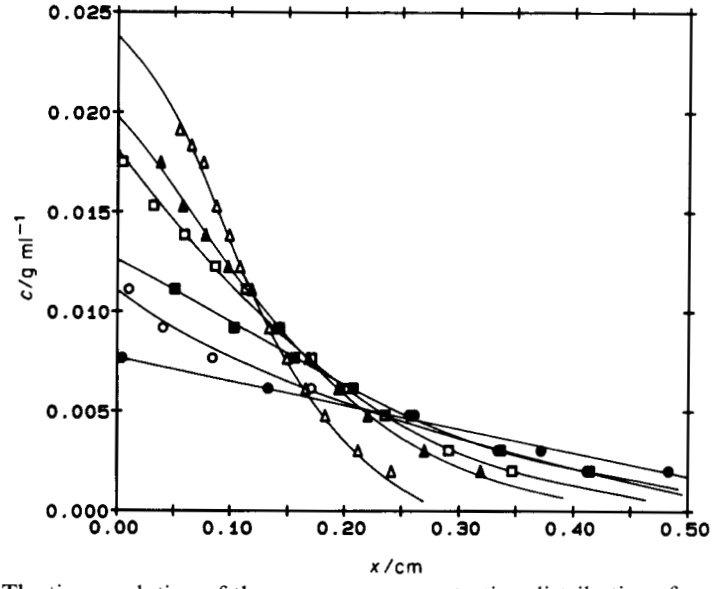

Figure 3. The time evolution of the c versus x concentration distributions from diffusion in the CB15/5CB system. ●, t = 20 600 s; ○, t = 40 700 s; ■, t = 55 100 s; □, t = 77 300 s; ▲, t = 134 900 s; △, t = 157 770 s.

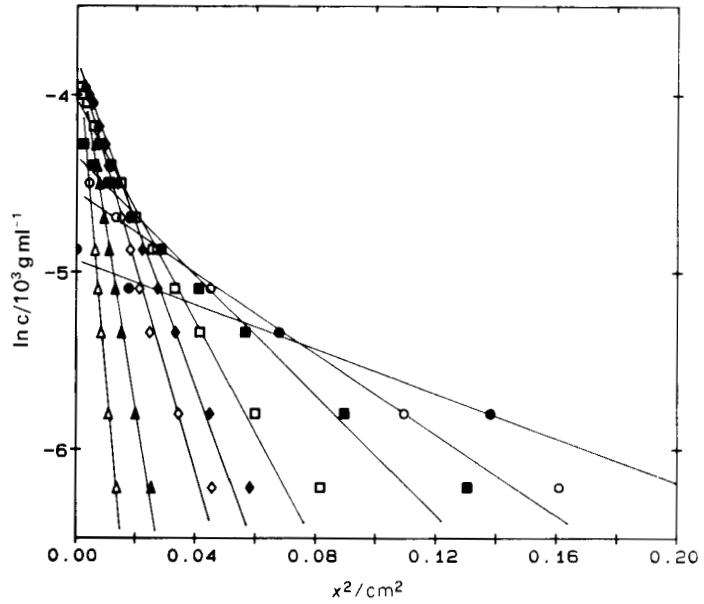

Figure 4. Time dependent plots of ln c versus x^2 from equation (6). D_{cx} values were determined from the linear slopes (see table). ●, t = 20 600 s; ○, t = 40 700 s; ■, t = 55 100 s; □, t = 77 300 s; ▲, t = 134 900 s; △, t = 157 770 s.

From equation (6), we have determined the D_{cx} values as a function of time from the typical ln [c] versus [x^2] plots. In figure 4, we show the dynamic evolution of the ln [c] versus [x^2] plots at different diffusion time scales. The results clearly show that the linear behaviour of the curves are in accord with equation (6). Note that in this

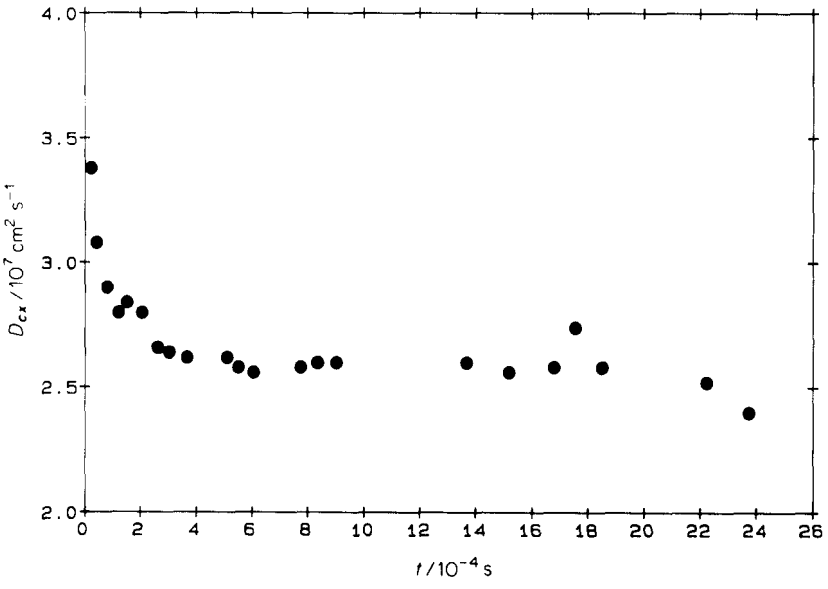

Figure 5. Time dependence of D_{cx} in the CB15/5CB system.

analysis D_{cx} is obtained as a function of the instantaneous time, but it is an integral value of both concentration and distance.

The calculated values of D_{cx} from the slopes of the plots in figure 4 are presented in figure 5 as a function of the diffusion time. These data indicate that within a shorter time scale the diffusion coefficient D_{cx} increases with the diffusion time, whereas above a characteristic time $t^* \approx (2 \times 10^4 \text{s})$, D_{cx} becomes time independent. The rational explanation of this result is that at the longer time scale (i.e. in the steady state) the diffusion coefficient is constant, whereas at the shorter time scale (i.e. in the non-steady state) the complex convective material flux in the non-linear region of mass transport leads to apparent variation of D_{cx} with time. Within the limits of the present experimental uncertainties, the average value of the D_{cx} at the plateau in figure 5 is $(2{\cdot}6 \pm 0{\cdot}1) \times 10^{-7}\,\text{cm}^2\,\text{s}^{-1}$. This average value is equivalent to the integral value of the mutual diffusion coefficient of the system, as represented by D in equations (2) and (5). Such correlation can also be obtained by integration of D_{cx} over the total experimental diffusion time (excluding the D_{cx} in the non-steady state region) according to

$$D = \langle D_{cx} \rangle = \int_{t^*}^{t'} D_{cx}\,dt \Big/ \int_{t^*}^{t'} dt. \tag{9}$$

Consequently, the dynamic analysis of the diffusion profile in the concentration–distance profile reveals two distinct diffusion regions of steady state and non-steady state which are separated by a characteristic time t^*. The significance of t^* is not yet known, but it is expected to be a property of the chemical structure, boundary condition and the temperature of the system.

5.2. *Diffusion coefficient versus distance*

Determination of the diffusion coefficient as a function of distance was carried out by the analysis of the diffusion profile on the c–t frame at constant distances from the

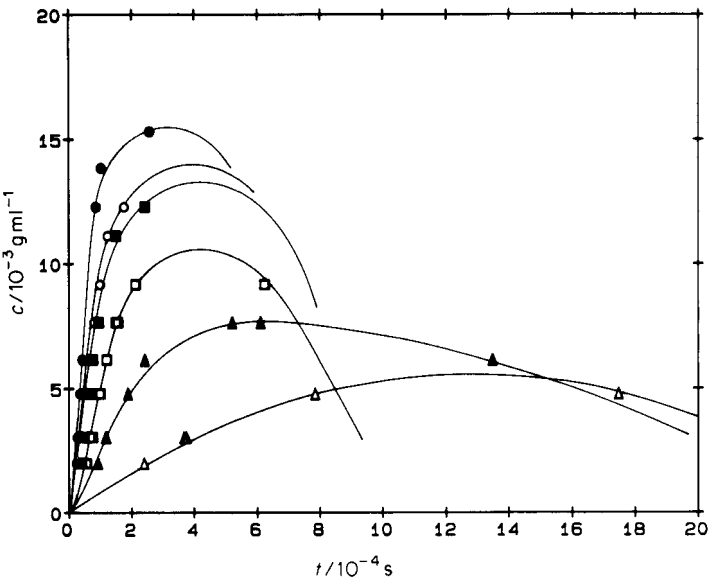

Figure 6. Spatial evolution of the c versus t concentration relaxations from diffusion in the CB15/5CB system. ●, t = 20 600 s; ○, t = 40 700 s; ■, t = 55 100 s; □, t = 77 300 s; ▲, t = 134 900 s; △, t = 157 770 s.

diffusion source (see figure 1). According to figure 2, the cross-sections of the c–x–t surface with planes parallel to the c–t plane should give curves as shown by the corresponding contour lines. In figure 6, we show the experimental plots of c versus t at various penetration distances in the CB15/5CB diffusion profile. Evaluation of the diffusion coefficient D_{ct} was carried out from the measurement of the slopes of the linear portions of the $\ln[c(t^{1/2})]$ versus $[t^{-1}]$ plots according to equation (7). The experimental results of D_{ct} as a function of the diffusion distance are shown in figure 7. The linear characteristics of the corresponding curves are in accord with equations (5) and (7) and with the present diffusion boundary condition. Again, notice that D_{ct} is instantaneous with x, but is an integral value of both c and t.

The relation between D_{ct} and x is presented in figure 8, which also indicates the existence of two diffusion regions separated by a characteristic distance x^* of $\sim 0{\cdot}1$ cm. At the shorter distance region below x^*, D_{ct} increases with distance, whereas above x^* it is independent of distance. In analogy with the time behaviour of D_{cx} in the previous section, we conclude that in steady state D_{ct} is spatially invariant giving an average value of $\langle D_{ct}\rangle = (2{\cdot}7 \pm 0{\cdot}1) \times 10^{-7}\,\mathrm{cm^2\,s^{-1}}$. The quantitative value of $\langle D_{ct}\rangle$ is in good agreement with $\langle D_{cx}\rangle$. This means that the spatial invariance of D_{ct} is also a measure of the average diffusion coefficient D (equations (2) and (5)). In fact the correlation between D and D_{ct} may be obtained from the spatial integration

$$D = \langle D_{ct}\rangle = \int_{x^*}^{x'} D_{ct}\,dx \Big/ \int_{x^*}^{x'} dx, \tag{10}$$

where x^* is the characteristic distance separating the steady state from the non-steady state diffusion. By neglecting the non-steady state, this integral will give a D_{ct} value equivalent to the average value obtained from the plateau value at the steady state (see figure 8).

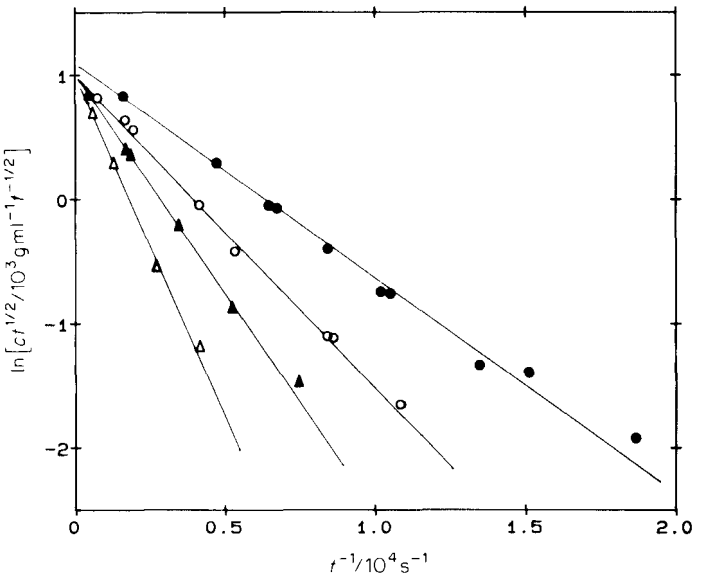

Figure 7. The spatial variation of $\ln[c(t)^{1/2}]$ versus $(t)^{-1}$ from equation (7). D_{ct} values were determined from the linear slopes (see table). ●, t = 20 600 s; ○, t = 40 700 s; ■, t = 55 100 s; □, t = 77 300 s; ▲, t = 134 900 s; △, t = 157 770 s.

Within the limits of the present experimental error, the time and space analyses of the diffusion surface gave invariant diffusion coefficients in steady state with the same average value. This value for the CB15/5CB system is $D = \langle D_{cx} \rangle = \langle D_{ct} \rangle = 2{\cdot}65 \times 10^{-7} cm^2 s^{-1}$. By an approximate calculation from the mobility concept (i.e. $D = x^2/2t$), assuming that $x^* = 0{\cdot}1$ cm and $t^* = 2 \times 10^4$ s, we find that at the onset of steady state diffusion, $D^* = 2{\cdot}5 \times 10^{-7} cm^2 s^{-1}$. This is in accord with the average diffusion coefficients from the c–x and c–t analyses, showing the analytical correlation between the brownian motion and fickian diffusion as a first order approximation approach.

5.3. *Diffusion coefficient versus concentration*

The dynamic study of the diffusion profile and determination of the diffusion coefficient from the x–t analysis of the cholesteric disclination lines have been reported for thermotropic systems [4 (c)–(e), 5, 6]. Recently this approach has been extended to lyotropic amphiphilic systems [7, 8]. The central assumption in the x–t diffusion analysis for the evaluation of D_{xt} is that the disclination lines (or the mid-distance between the disclination lines) are the optical manifestations of small volume elements with constant solute concentration. The differential concentration within each disclination (or mid-distance disclination) line is quantitatively manifested by a local pitch value of p_k or $p_{k-1,k}$. Therefore, the space–time trajectory of the disclination lines is the brownian motion manifestation of fickian diffusion. In other words, the diffusive motion of the disclination lines (see figure 1) can be considered as the brownian particles which are subject to a bulk concentration gradient force field. This analogy will not affect the outcome of the analysis of the diffusion data, because the mathematical solution of the semi-infinite boundary condition (equation (5)) is the same in both brownian motion and fickian diffusion. In fact, equation (8) indicates that the

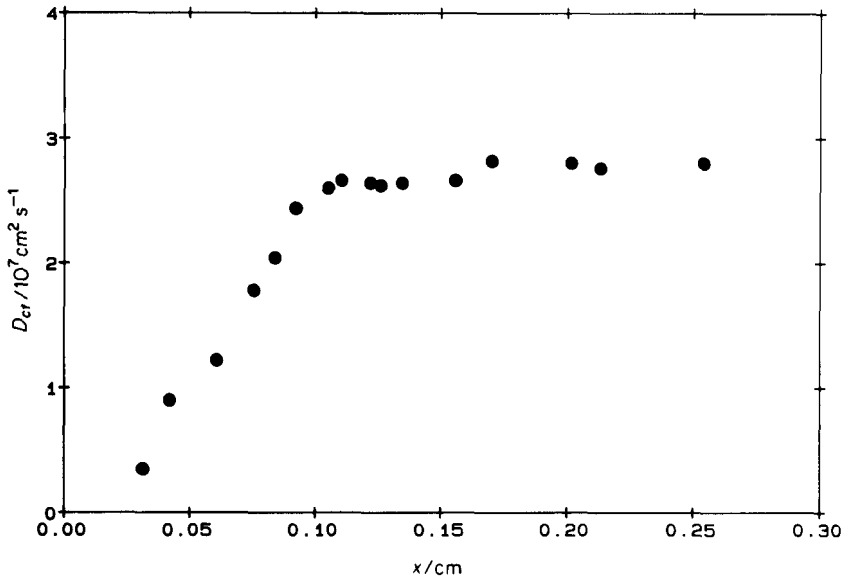

Figure 8. Distance dependence of D_{ct} in the CB15/5CB system.

cross-sections of the c–x–t diffusion surface with planes parallel to the x–t plane should give linear plots of $[x^2/t]$ versus $\ln[t]$, where D_{xt} could be determined from the corresponding linear slopes.

In figure 9, we show the space–time trajectories of the individual p_k and $p_{k-1,k}$, for the CB15/5CB system. In order to keep the notation as simple as possible, we use c instead of c_k or p_k throughout this section (see also the table). The convergence of the x–t trajectories can be explained from the gaussian relaxation behaviours at constant concentrations. In figure 10 we show the $[x^2/t]$ versus $\ln[t]$ plots for the experimental data of figure 9. In the longer time region, these curves exhibit linear behaviour with negative slopes (in accord with equation (8)). From the slopes of these lines, we have evaluated the D_{xt} values attributed to the differential concentrations in the diffusion profile. These values are also tabulated in the table.

The data of figure 10 also indicate that regardless of the c, the space–time profile for each c is divided into two distinct regions. The long-time region attributed to the steady state diffusion is governed by the second term in the right-hand side of equation (8) (sections with negative slopes). The short-time regions exhibit non-steady state diffusion that their positive functional behaviour is dominated by the first term in the right-hand side of equation (8). In order to verify the validity of this analogy and to examine the behaviour of D_{xt} in the whole space–time frame, we have performed a computer curve fitting procedure to the experimental data. In this respect, equation (8) was rearranged to the form

$$x = [At - Bt\ln(t)]^{1/2}, \tag{11}$$

where

$$A = D_{xt}\ln[M/C(\pi D_{xt})^{1/2}]$$

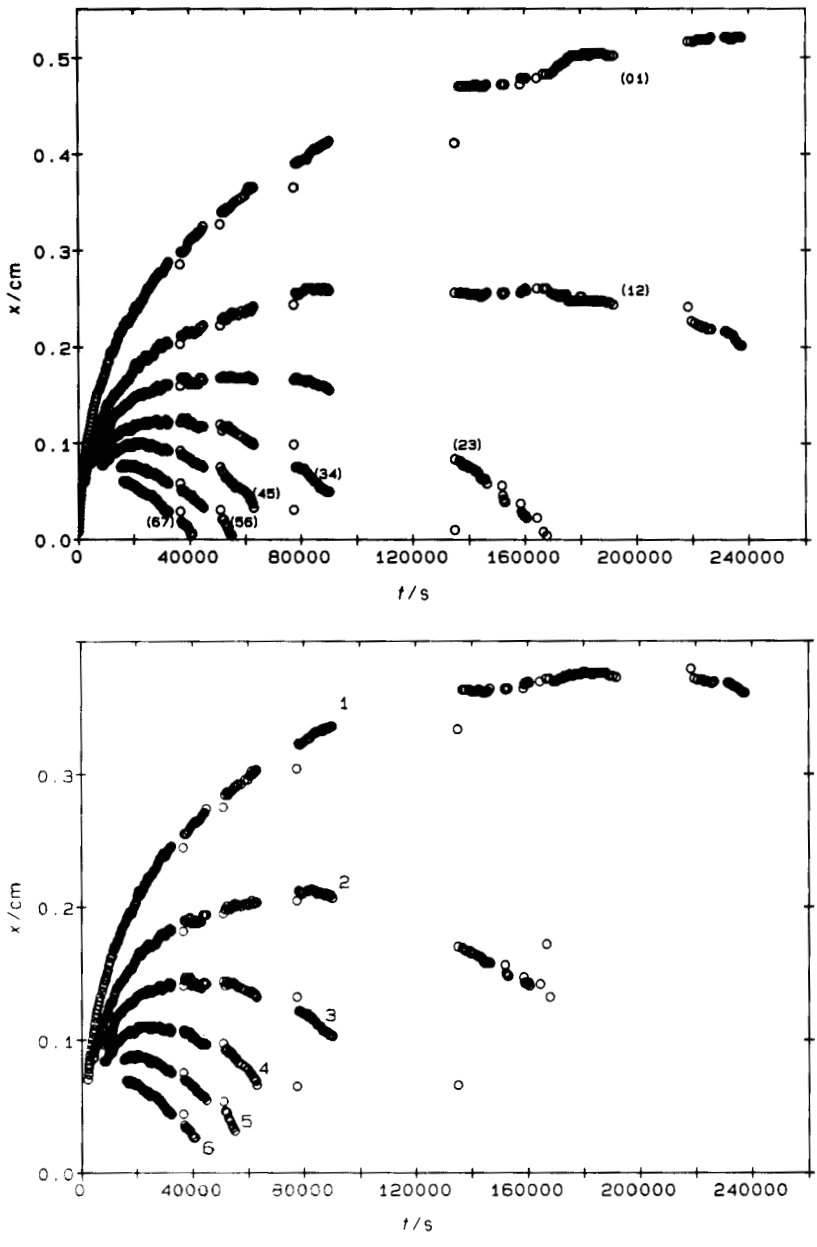

Figure 9. Space–time trajectories of the disclination lines (bottom) and their mid-distances (top) in the diffusion profile of CB15/5CB (see figure 1).

and

$$B = 2D_{xt}.$$

Equation (11) was fitted to the individual curves of figure 9 at successive diffusion times, and the corresponding D_{xt} values were evaluated from the B parameter. The results as shown by two examples in figure 11 indicate that in all concentrations, the D_{xt}

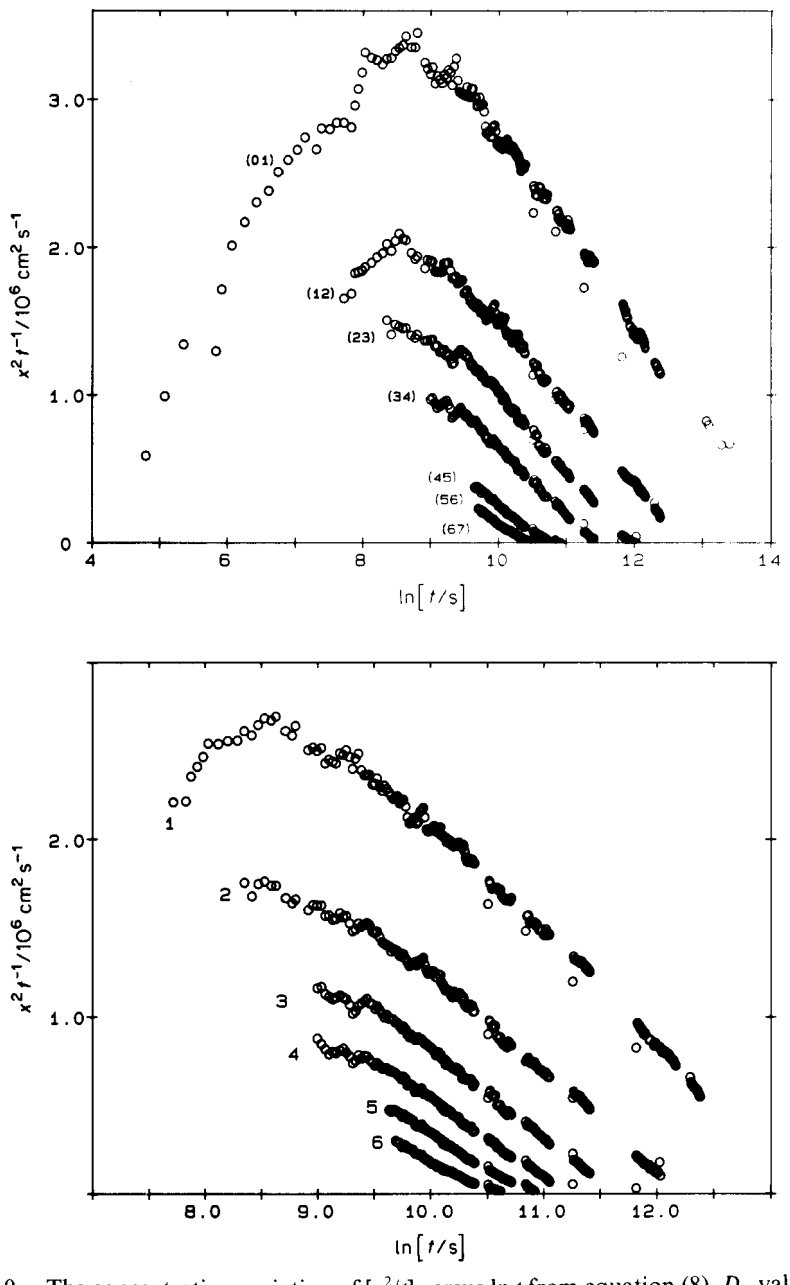

Figure 10. The concentration variation of $[x^2/t]$ versus $\ln t$ from equation (8). D_{xt} values were determined from the linear slopes (see table).

first increases with diffusion time becomes independent of time in the long-time regime. The time independence of D_{xt} is identical to those obtained from the slope measurements. Accordingly, we found excellent agreements between D_{xt} values obtained from the curve fitting and the slope measurements (see table). The poor agreement between the data at the higher concentration range is due to the lack of x–t trajectory data in the short-time region which provides poor curve fitting results. In

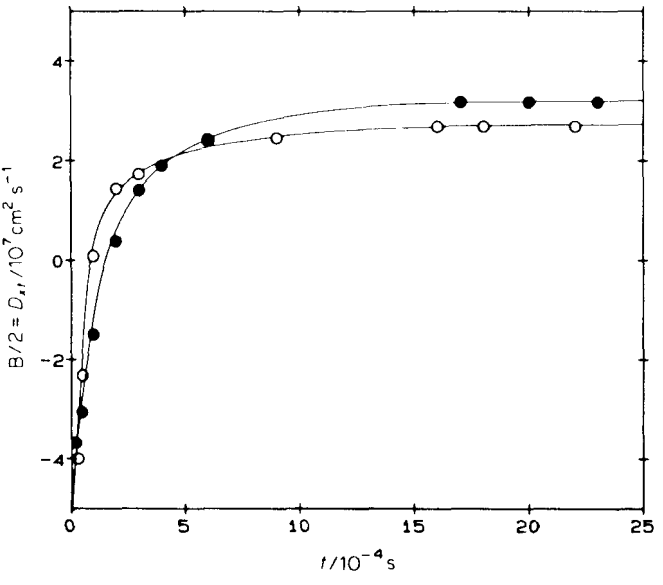

Figure 11. The time dependence of D_{xt} obtained from the curve fitting procedure for two disclination lines (see equation (11)).

such cases, the D_{xt} values from the slope measurements are more reliable. From these results, we confirm that the D_{xt} determined from the slopes of the $[x^2/t]$ versus ln t plots are indeed obtained in the steady state diffusion and are independent of the space–time coordinates.

The concentration dependence of all diffusion data is shown in figure 12. Note that the reported D_{xt} values are only from the slope measurements (see table 1). The concentration dependence of D_{xt} is apparently a linear relation. Since the molecular weights of the CB15 and 5CB are identical (MW = 249), the concentration dependence of D_{xt} must be due to the steric effect arising from the difference in their molecular shape and volume. Note that in an ideal situation where the molecular structure of the solute and solvent are identical, the concentration should not affect the D_{xt} value (i.e. the D_{xt} versus c curve should be a horizontal line). Although D_{xt} can be closely related to the self-diffusion coefficients at various concentrations of the CB15/5CB mixture, a more realistic condition for the study of self-diffusion in these systems can be achieved by the use of a solute and solvent with identical chemical structures [3 (b)].

The effect of the molecular structure of the solute on the concentration dependence of the diffusion coefficient was further explored by incorporating the diffusion data of cholesteryl oleylcarbonate (COC/5CB) system [8], by correcting the D_{xt} values for the mass effect [2]. Note that the molecular weight of COC (MW = 681) is about 2·5 times larger than for 5CB. A comparison between the concentration dependence of D_{xt} values in the COC/5CB and CB15/5CB systems in figure 12 clearly indicates that, in the absence of the mass effect, the D_{xt} of COC/5CB are significantly smaller than those for the CB15/5CB system. The origin of the non-linear behaviour of D_{xt} in the COC/5CB system may be due to the contribution of the cholesteric pitch (originated by the mesophase–surface interactions) to the diffusion coefficient values. This is a reasonable speculation, because as we see in figure 11, the effective non-linearity of the D_{xt} data at higher concentrations (or lower pitch values) in both

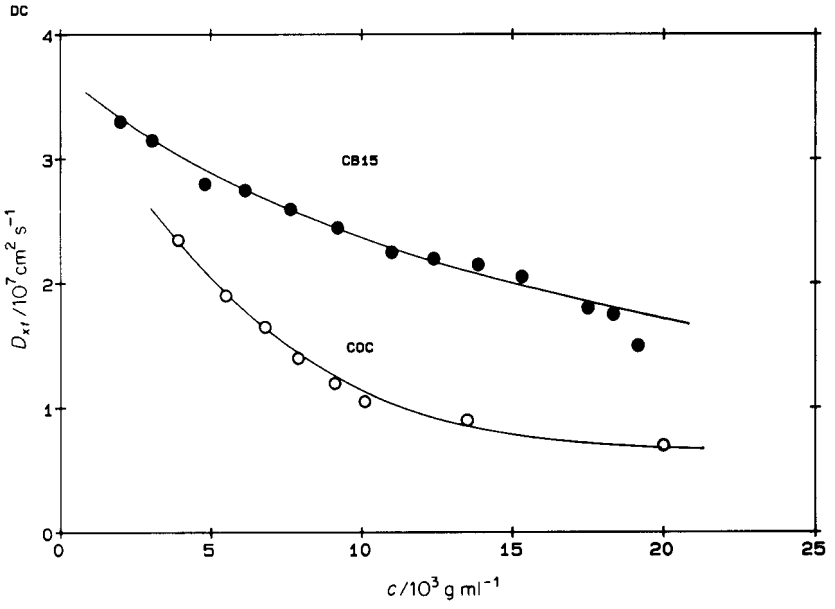

Figure 12. Concentration dependence of D_{xt} in CB15/5CB (filled circles) and COC/5CB (open circles) mixtures. ○, $k = 0,1$); ●, $k = (1,2)$.

systems could be attributed to the contributions of the larger twist elastic energies of smaller pitch values. Furthermore, by acknowledging that the effect of the concentration gradient is negligible, D_{xt} can be closely related to the apparent self-diffusion coefficient of the system in each concentration. Accordingly, we evaluated the self-diffusion coefficient for the pure 5CB solvent by extrapolation of the D_{xt}–c data to $c = 0$. In this extrapolation procedure, polynomial functions of the second degrees were fitted to the diffusion data of the CB15/5CB and COC/5CB systems giving:

$$\text{CB15/5CB: } D_{xt}/\text{cm}^2\,\text{s}^{-1} = (3{\cdot}4 \times 10^{-7}) - (1{\cdot}2 \times 10^{-5} c/10^3\,\text{g ml}^{-1}) + (1{\cdot}2) \times 10^{-4})(c/10^3\,\text{g ml}^{-1})^2,$$

$$\text{COC/5CB: } D_{xt}/\text{cm}^2\,\text{s}^{-1} = (3{\cdot}4 \times 10^{-7}) - (3{\cdot}3 \times 10^{-5})(c/10^3\,\text{g ml}^{-1}) + (9{\cdot}6 \times 10^{-4})(c/10^3\,\text{g ml}^{-1})^2.$$

At $c = 0$, the first terms on the right-hand sides of the above relations give the same values for the self-diffusion coefficient for pure 5CB; i.e. $D_s(5\text{CB}) = 3{\cdot}4 \times 10^{-7}\,\text{cm}^2\,\text{s}^{-1}$. Note that the difference between D_s (5CB) in this study and the values reported previously is due to the inappropriate mass correction approach used [4].

The average diffusion coefficient D of the system can also be obtained by integration of D_{xt} over the entire concentration range of the diffusion profile according to

$$D = \langle D_{xt} \rangle = [1/C_0] \int_0^{C_0} D_{xt}\,dc, \tag{12}$$

where C_0 is the initial concentration of the diffusing solute (see table 1). In practice,

however, since the values of D_{xt} are not known in the very dilute region of concentration, the integral of equation (12) was replaced by the approximate summation

$$\langle D_{xt} \rangle = [(\Sigma D_n C_n)/C_0] = 2{\cdot}1 \times 10^{-7} \text{cm}^2 \text{s}^{-1},$$

where D_n and c_n are the corresponding D_{xt} and c values for $n = 1$–13 experimental data. Within the limits of the present experimental error, the evaluated $\langle D_{xt} \rangle$ is in close agreement with the $\langle D_{cx} \rangle$ and $\langle D_{ct} \rangle$ values obtained in §§5.1 and 5.2.

6. Conclusions

In the present analytical approach, we used the unique features of the OMMT technique and made a detailed analysis of the diffusion profile in a binary liquid-crystalline system. We analysed the c–x–t diffusion surface in three individual experimental coordinate frames, and determined the corresponding values of instantaneous and integral diffusion coefficients. The average values of the diffusion coefficients from the steady state region were invarient with respect to space and time, whereas the diffusion coefficients in the non-steady state were dependent on both time and distance. From the space–time analysis of the diffusion profile, we determined the concentration dependence of the mutual diffusion coefficient of the system. The present experimental method provides a comprehensive analysis of the steady state diffusion, as well as information on the non-steady state region, which cannot be achieved by conventional mass transport techniques.

References

[1] Tyrrel, H. J. V., and Harris, R. K., 1984, *Diffusion in Liquids* (Butterworths).
[2] Crank, H., 1956, *The Mathematics of Diffusion* (Oxford University Press).
[3] Hakemi, H., and Labes, M. M., (a) 1974, *J. chem. Phys.*, **61**, 4020; (b) 1975, *Ibid*, **63**, 3708.
[4] Hakemi, H., (a) 1982, *J. appl. Phys.*, **53**, 5333; (b) 1982, *Molec. Crystals liq. Crystals Lett.*, **82**, 303; (c) 1983, *J. chem. Phys.*, **79**, 1434; (d) 1983, *Physics Lett.* A, **95**, 35; (e) 1983, *Molec. Crystals liq. Crystals*, **95**, 309.
[5] Hakemi, H., and Krigbaum, W. R., 1985, *J. Polym. Sci. Polym. Phys. Ed.*, **23**, 253.
[6] Hakemi, H., 1986, *J. Polym. Sci. Lett. Ed.*, **24**, 377.
[7] Hakemi, H., Varanasi, P. P., and Tcheurekfjian, N., 1987, *J. phys. Chem.*, **91**, 120.
[8] Hakemi, H., Varanasi, P. P., and Chang, Q., 1988, *J. phys. Chem.* (submitted).
[9] De Gennes, P. G., 1974, *The Physics of Liquid Crystals* (Oxford University Press).
[10] Kassubek, P., and Meier, G., 1972, *Liquid Crystals* Vol. 7, Part II, edited by G. H. Brown (Gordon & Breach), p. 753.
[11] Hakemi, H., and Varanasi, P. P., 1986, *Liq. Crystals*, **1**, 63.